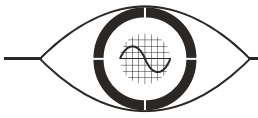

Lehrstuhl für Bildverarbeitung
Institute of Imaging & Computer Vision

Fuzzy Pulmonary Vessel Segmentation in Contrast Enhanced CT data

Jens N. Kaftan and Atilla P. Kiraly and Annemarie Bakai and Marco Das and Carol L. Novak and Til Aach

Institute of Imaging and Computer Vision
RWTH Aachen University, 52056 Aachen, Germany
tel: +49 241 80 27860, fax: +49 241 80 22200
web: www.lfb.rwth-aachen.de

in: Medical Imaging 2008: Image Processing. See also BibTeX entry below.

BibTeX:

```
@inproceedings{KAF08b,
  author    = {Jens N. Kaftan and Atilla P. Kiraly and Annemarie Bakai
   and Marco Das and Carol L. Novak and Til Aach},
  title     = {{F}uzzy {P}ulmonary {V}essel {S}egmentation in {C}ontrast {E}nhanced {CT} data},
  booktitle = {Medical Imaging 2008: Image Processing},
  editor    = {J. M. Reinhardt and J. P. W.Pluim},
  publisher = {SPIE},
  volume    = {6914},
  address   = {San Diego, USA},
  month     = {February 16--21},
  year      = {2008},
  pages     = {69141Q-1--12}}
```


document created on: March 23, 2008
created from file: lungvesselsegmentation.tex
cover page automatically created with CoverPage.sty
(available at your favourite CTAN mirror)

RWTH AACHEN
RHEINISCH-WESTFÄLISCHE TECHNISCHE HOCHSCHULE AACHEN

Fuzzy Pulmonary Vessel Segmentation in Contrast Enhanced CT Data

Jens N. Kaftan[ab], Atilla P. Kiraly[c], Annemarie Bakai[b],
Marco Das[d], Carol L. Novak[c], and Til Aach[a]

[a]Institute of Imaging and Computer Vision, RWTH Aachen University,
Templergraben 55, 52056 Aachen, Germany
[b]Siemens Medical Solutions, Siemensstr. 1, 91301 Forchheim, Germany
[c]Siemens Corporate Research, 755 College Road East, Princeton, NJ 08540, USA
[d]Department of Diagnostic Radiology, RWTH Aachen University Hospital,
Pauwelstr. 30, 52074 Aachen, Germany

ABSTRACT

Pulmonary vascular tree segmentation has numerous applications in medical imaging and computer-aided diagnosis (CAD), including detection and visualization of pulmonary emboli (PE), improved lung nodule detection, and quantitative vessel analysis. We present a novel approach to pulmonary vessel segmentation based on a fuzzy segmentation concept, combining the strengths of both threshold and seed point based methods. The lungs of the original image are first segmented and a threshold-based approach identifies core vessel components with a high specificity. These components are then used to automatically identify reliable seed points for a fuzzy seed point based segmentation method, namely fuzzy connectedness. The output of the method consists of the probability of each voxel belonging to the vascular tree. Hence, our method provides the possibility to adjust the sensitivity/specificity of the segmentation result *a posteriori* according to application-specific requirements, through definition of a minimum vessel-probability required to classify a voxel as belonging to the vascular tree.

The method has been evaluated on contrast-enhanced thoracic CT scans from clinical PE cases and demonstrates overall promising results. For quantitative validation we compare the segmentation results to randomly selected, semi-automatically segmented sub-volumes and present the resulting receiver operating characteristic (ROC) curves. Although we focus on contrast enhanced chest CT data, the method can be generalized to other regions of the body as well as to different imaging modalities.

Keywords: segmentation, pulmonary vessel, chest CT, fuzzy connectedness

1. INTRODUCTION

Pulmonary vascular tree segmentation is the fundamental basis for different medical applications, such as the detection and visualization of pulmonary emboli (PE), improved lung nodule detection, or quantitative vessel analysis. Different applications have varying requirements. For example, in PE applications, vessels beyond the subsegmental level have minimal impact on patient prognosis and are usually not of interest. In quantitative analysis of smaller vessels, accurate segmentation of vessel edges is the primary requirement. Additionally, the correct reproduction of the vascular topology is important for certain artery-vein separation methods. In general, a more comprehensive segmentation is of benefit. Difficulties in achieving a correct segmentation include partial volume effects and high density airway walls, which can be confused with vessels.

Typical pulmonary vessel segmentation approaches in computed tomography (CT) scans vary from threshold operations to front propagation techniques, using either original or filtered data [1–7].

The method presented in [1] segments the lung vessels in contrast enhanced CT data by first applying a threshold operation to the lung areas. Regions above a certain threshold are analyzed by a connected component

Further author information: (Send correspondence to J. N. Kaftan)
E-mail: jens.kaftan@lfb.rwth-aachen.de, Telephone: +49 241 80 27974

labeling method. Small components are eliminated and the remaining components are analyzed by a centerline model to eliminate small diameter vessels. To improve the specificity of automated lung nodule detection in thoracic CT scans, Wu et al. [2] propose a vessel extraction approach that uses locally adaptive thresholds, which are automatically determined based on the local neighborhood. The result is used to build fuzzy spherical objects representing the vessels, using regulated morphological operations. Finally, a tracking algorithm is used to connect these objects to a tree structure.

Other methods often utilize vessel enhancement filters, such as the line-filter proposed by Frangi et al. [8] or Sato et al. [9], and demonstrated, e.g., in [3]. These methods utilize eigenvalues of the Hessian matrix computed from first and second order derivatives of the image, and formulate them into a final value. The method presented in [3] determines an initial segmentation by thresholding the filtered output. To fill resulting gaps, especially at bifurcations, which usually do not have a high response to line-filters, a tracking algorithm [10] is used. The authors of [4] also designed a filter response function, based on the eigenvalues of the Hessian matrix, which was designed to enhance vessels as well as vessel bifurcations and to suppress non-vessel structures. Hierarchical expectation-maximization (EM) was then applied to segment the vessels, by extracting the high response voxels at each scale.

Alternatively seed-point based algorithms, such as region growing techniques (see, e.g., [11]) or fast marching techniques (see, e.g., [5]) can be applied. The method used by [5] starts a front propagation process from one or more seed positions with the front propagation velocity kept constant to segment the pulmonary vessel tree from multi-slice CT datasets. In this case, the propagation process is comparable to region growing. Additionally, bifurcation points are detected during segmentation by checking the propagation front for connectedness, which is equivalent to the branch-based region growing approach [11]. Branches whose radii exceed a maximally allowed value (indicating leakage), are rejected. Zhou et al. [6] extract an initial pulmonary vessel tree by a threshold based region growing method from multi-slice chest CT images without any contrast enhancement. The segmentation result is refined based on a branch-by-branch analysis. In addition, voxels in close proximity to the airway surface are disregarded as the bronchial wall. Zhang et al. [7] propose to use level set methods to extract pulmonary vessels from CT data. In their framework, they combine edge and region-based speed terms to model the front propagation in a multiscale space.

These algorithms usually limit themselves to the lungs as the region of interest (ROI). Although threshold-based approaches are very fast, using a threshold alone completely disregards local connectivity information. As a result, isolated false positive regions might be included in the segmentation output, and structures that should be connected might be separated, thus leading to incorrect interpretation of the data.

In contrast, seed-point based approaches rely on local connectivity. However, depending on the accuracy of the lung segmentation method, the arterial and venous tree inside the lung region might already be divided into several sub-trees. This is because major blood vessels close to the hilum are often not included in the lung segmentation, thus requiring multiple seed points. In addition, local inhomogeneities, such as those caused by emboli, might cause an early termination of the growing process. As a result, complete subtrees might be missed during segmentation. Filter-based approaches involving the Hessian matrix or EM methods frequently need multiple scales to capture all vessel details. Coupling this necessity with the multiple computations required for each scale tends to make these methods rather computationally intense and therefore slow.

However, different applications have different requirements for segmentation sensitivity and specificity. For instance, computer-aided diagnosis (CAD) applications for PE detection [12] require that all arteries up to a certain level are included with high sensitivitiy, since each missed artery is not accessible for the detection step. In contrast, CAD applications for automatic lung nodule detection often utilize a pulmonary vessel segmentation to reduce the number of false positives [13], hence requiring a high vessel segmentation specificity.

We present fully- and semi-automatic methods for the segmentation of pulmonary vessels in contrast enhanced CT images. Our algorithms combine the strengths of both threshold and seed-point based methods by first identifying multiple seed points with a high specificity and then continuously adding neighboring voxels based on the strength of connectivity. The result is a fuzzy segmentation that can be adapted to the sensitivity/specificity of the application requirements.

2. METHODS

Our method consists of two principal phases as shown in the flowchart in Figure 1. The original contrast enhanced CT image along with a segmentation of the left and right lungs (see Section 2.1) are used as input.

The first phase identifies the core components of the vascular tree within the lung areas with a high specificity. This step performs an initial segmentation using a threshold-based approach as described in Section 2.2. Depending upon the chosen parameters, this step can identify many connected regions or just a few. Subsequently each region is reduced to one or more seed positions. This has the advantage that different subtrees, if present, can be detected by this step. Moreover, in the presence of a PE within a larger artery, the successor subtrees might be identified separately as long as the PE is non-blocking. This means that even if a PE causes a seed-point based segmentation algorithm to terminate early, the descendant subtrees are not completely lost during the segmentation process. Note that the seed position extraction step is designed to identify seeds that tend to be located towards the center of the lungs, i.e., towards the root of each sub-tree.

The second processing phase creates an improved fuzzy segmentation using the original data along with the identified seed positions, which is described in detail in Section 2.3. Assuming the seed positions are located inside the pulmonary vessels, the probability that a voxel also belongs to the vascular tree is determined by examining the paths between the voxel of interest and the seed positions. Hence, this phase results in a vessel probability map. If necessary, this step might be repeated, guided by user interventions (see Section 2.4). Finally, the binary segmentation is obtained by applying a threshold to the probability values, allowing the sensitivity of the method to be adjusted a posteriori in this last step.

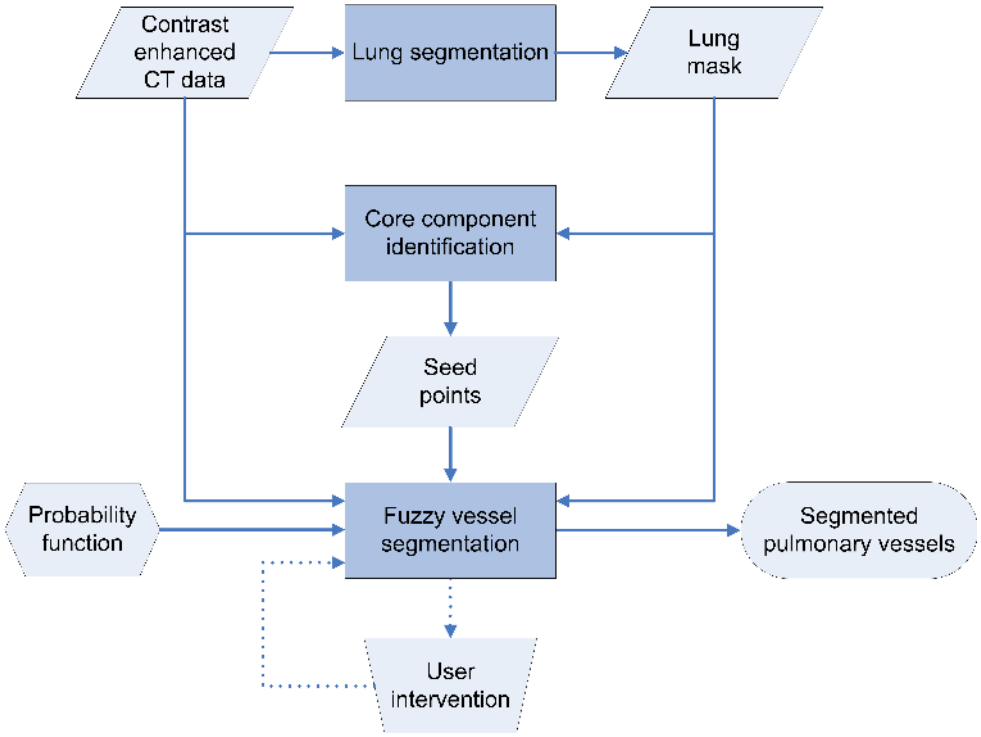

Figure 1. A high-level diagram of the steps and output of the proposed method. The input consists of the original, contrast enhanced CT data. A lung segmentation method is applied to identify the left and right lung as the ROIs. The core component identification step is then used to automatically identify seed points within the core lung vessels. These are used along with a probability function as input to the fuzzy vessel segmentation step. If necessary, this step might be repeated, guided by user interventions. The final output is then the segmentation of the pulmonary vessels within the lung mask.

2.1 Lung Segmentation

Lung segmentation is an important pre-processing step for different applications, e.g., the detection of lung nodules or pleura mesothelioma, parenchyma analysis, and pulmonary vessel extraction. While some applications, like pleura mesothelioma detection, require an accurate outline of the pleura wall, other applications, such as pulmonary vessel segmentation, do not have such rigorous requirements on the segmentation accuracy. Although the lung mask is only intended to limit the segmentation step to the lung regions as the ROI, the prevention of ribs or other bright structures near the lung surface from being included into the lung mask potentially increases the specificity of a later vessel segmentation step.

The lung segmentation step used by our system initially separates body from non-body regions using a threshold T^i, which is determined iteratively [14]:

$$T^{i+1} = \frac{\mu_b + \mu_n}{2} \tag{1}$$

where μ_b and μ_n correspond to the mean gray value of the body voxels and non-body voxels, respectively, after segmentation with threshold T^i. The initial threshold is set to $T^0 = -500$ HU and the threshold update procedure is repeated until the estimated threshold converges, i.e., $T^{i+1} = T^i$. Then, a seed point is automatically selected in the trachea, by searching for a connected region of a certain size, close to the origin of the image within the top slices of the resulting binary mask.

Afterwards, region growing is performed from this seed position, once on the binary mask in order to fill the lungs, and once with adaptive thresholds [15] on the original data to segment the major airways. The resulting airway segmentation is then subtracted from the resulting lung segmentation to remove the trachea and major airways. Note that the airway segmentation can also be used at a later point to prevent airway walls from being included in the vessel segmentation as described in Section 2.3.2. Finally, morphological closing, i.e., dilation followed by erosion, is performed on the segmented image to fill empty spaces caused by, e.g., blood vessels. The erosion operator is chosen to be slightly larger than the dilation operator to prevent ribs or other structures near the lung surface, such as the Superior Vena Cava (SVC), from being included in the lung mask. This, however, does not limit the performance of a later vessel segmentation step, since vessels can typically only be seen $5-10$ mm from the pleura wall in normal CT scans [16]. The resulting lung segmentation is exemplarily shown in Figure 2.

(a) Axial view (b) Volume rendering

Figure 2. Lung segmentation using the proposed method. Figure (a) shows the result delineated as a contour (yellow) in an axial view. The complete segmentation result is visualized using 3D rendering techniques in (b).

2.2 Core Component Identification

To identify reliable seed positions within the lung vessels, the core vessel components are first extracted from the masked input data, in a manner similar to the vessel segmentation method described in [1]. A threshold with "conservative" boundaries, e.g., $T_{\min} = 200$ HU, is applied to the lung regions to create an initial segmentation with a high specificity. Thus voxels identified at this early stage most likely belong to the vascular tree. To eliminate further false positive regions, a connected-component labeling is performed on the segmented structures. Components that do not exceed a minimal volume $V_{\min}$ in size, e.g., $V_{\min} = 500$ voxels, are eliminated. Small holes within this segmentation output are closed using morphological operations. Compared to [1], the parameters are chosen to obtain a core segmentation with a very high specificity, rather than a segmentation of a complete tree structure (see Fig. 3a-b).

Next, the segmented components are converted into a structure that reflects the likelihood of centerlines C, based on a 3D Euclidean distance transform. Voxels within the segmentation output with a higher distance to the closest vessel surface are located further inside the vessels and hence are more likely to correspond to the centerline (see Fig. 3c). That means that local maxima within such a structure most likely correspond to the centerline, and that the associated distance value corresponds to a radius estimate. Hence local maxima within a kernel window of size $5 \times 5 \times 5$ voxels, and where the radius estimate is within the range of radii of interest, e.g., $[r_1, r_2] = \left[\sqrt{2}, \infty\right] \cdot$ voxelsize, become seed point candidates.

Depending upon the physical location and the radius estimates, these seed candidates are clustered together, designating seed positions with a large value of r as cluster representatives. That means that the cluster representatives, which are the final seed positions for the methods described in Section 2.3, tend to be located towards the origin of each component, since the radius estimates are maximal in that area. Therefore, starting with the seed candidate with maximum radius estimate, we assign each further seed candidate within a certain distance to the same group. In particular, two seed candidates $\mathbf{s}_1$ and $\mathbf{s}_2$ are grouped together if the Euclidean distance $d(\mathbf{s}_1, \mathbf{s}_2)$ is smaller than the sum of the radius estimates at both positions, i.e., if

$$d(\mathbf{s}_1, \mathbf{s}_2) < (r(\mathbf{s}_1) + r(\mathbf{s}_2)) \tag{2}$$

This is continued until all seed candidates are assigned to one group, while a considered point that was not yet assigned to another candidate, will found a new group. Finally, for each group, the seed candidate with the largest radius estimate is chosen as cluster representative. The number N of detected seed points, however, depends on the chosen parameters. In the case that one component misleadingly includes arteries and veins (which have been connected due to misinterpretation because of, e.g., partial volume effects), different seed-points within the arterial and venous subtrees were most likely chosen as long as their origins differ distinctly within the initial segmentation.

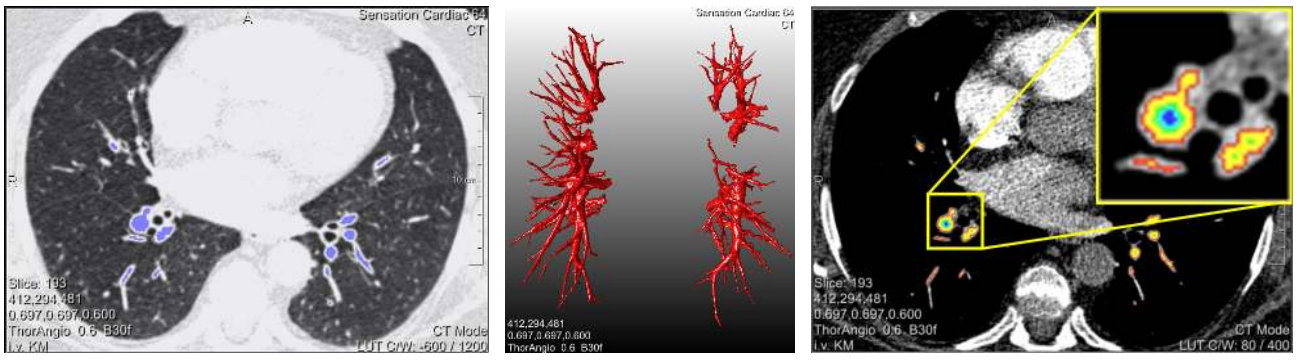

(a) Axial view (b) Volume rendering (c) Distant transformed

Figure 3. Core vessel segmentation as overlay to an axial view (a) and using volume rendering techniques (b). For each voxel within the segmentation result, the minimal 3D Euclidean distance to the vessel surface has been calculated and is shown color coded in (c).

2.3 Fuzzy Vessel Segmentation

After multiple seed points throughout the whole lung have been identified, they are used for a seed-point based segmentation approach. Assuming all seed points are located within the vascular tree, we create a probability map where the belongingness of each voxel to one of the seed points and hence to the class "vessel" is stored, using the masked CT data along with the identified seed positions from Section 2.2. Finally, this probability map is converted into a binary segmentation mask by applying a threshold, depending on the application-specific requirements.

To calculate such a probability measure, the vessel probability of each seed position is first set to one. Next, starting from the seed positions, neighboring voxels receive a vessel probability based on local image features and the probability measure of their neighbors, while those not visited have a vessel probability of zero. This is repeated in an iterative fashion, where voxels with a high probability are processed first, until the probability that a newly visited voxel belongs to one of the seed positions drops below a specified value. Thus, the process can be compared to a front evolution or region growing process, where neighboring voxels that are more likely to belong to a vessel are added earlier than unlikely ones.

This general description is realized by the fuzzy connectedness algorithm, which has already been successfully applied to quantifying multiple sclerosis lesions of the brain [17], vessel segmentation in magnetic resonance angiography (MRA) [17], and airway segmentation in CT [18]. The method is described in detail in the following section.

2.3.1 Fuzzy Connectedness

Using the fuzzy connectedness algorithm [19], a probability measure that a voxel belongs to one of the seed-points is assigned to each voxel based on dynamic programming, using a probability function (see Section 2.3.2), which models the so-called "hanging togetherness" of voxels within the scene.

An object O with its seed positions $\mathbf{s}_i \in \mathbb{O},\ i \in [0, N-1]$ and the background B are separated by dividing the set of voxels present in the scene in such a way, that the "hanging togetherness" or "belongingness" of each object voxel to $\mathbb{O}$ is larger than the "belongingness" of each background voxel. Note that the background itself might consist of objects in which we are not interested. Here, the set of voxels corresponds to the voxels described by the lung mask and the seed positions $\mathbf{s}_i$ are defined by the output of Section 2.2.

The probability that two neighboring voxels $\mathbf{c}, \mathbf{d}$ belong to the same group is therefore defined by a local fuzzy relation called "affinity" $\mu_\kappa(\mathbf{c}, \mathbf{d})$. The neighborhood of a voxel in 3D data is typically defined either by its 6- or 26- nearest neighbors. The affinity of non-neighboring voxels equals zero and the affinity of a voxel to itself equals one: $\mu_\kappa(\mathbf{c}, \mathbf{c}) = 1$. For all other pairs of voxels the affinity is defined by a probability function as described in Section 2.3.2. The local affinity is designed to be symmetric, i.e.,

$$\mu_\kappa(\mathbf{c}, \mathbf{d}) = \mu_\kappa(\mathbf{d}, \mathbf{c}) \tag{3}$$

The "strength of connectedness" of two distant voxels $\mathbf{c}, \mathbf{d}$ along a certain path $p_{\mathbf{c},\mathbf{d}}$ within the scene is simply the smallest pairwise fuzzy affinity along this path, while the path $p_{\mathbf{c},\mathbf{d}}$ from $\mathbf{c}$ to $\mathbf{d}$ is a sequence of $m > 2$ neighboring voxels $\left\langle \mathbf{c}^{(1)}, \mathbf{c}^{(2)}, ..., \mathbf{c}^{(m)} \right\rangle$, such that $\mathbf{c}^{(1)} = \mathbf{c}$ and $\mathbf{c}^{(m)} = \mathbf{d}$. Thus the "strength of connectedness" equals:

$$\mu_N(p_{\mathbf{c},\mathbf{d}}) = \min \left[\mu_\kappa(\mathbf{c}^{(1)}, \mathbf{c}^{(2)}), \mu_\kappa(\mathbf{c}^{(2)}, \mathbf{c}^{(3)}), ..., \mu_\kappa(\mathbf{c}^{(m-1)}, \mathbf{c}^{(m)}) \right] \tag{4}$$

As there are various possible paths connecting $\mathbf{c}$ and $\mathbf{d}$, the global connectivity $\mu_K(\mathbf{c}, \mathbf{d})$ is defined as the largest of the strengths of connectedness of all possible paths between $\mathbf{c}, \mathbf{d}$:

$$\mu_K(\mathbf{c}, \mathbf{d}) = \max_{p_j \in \mathbb{P}_{\mathbf{c},\mathbf{d}}} \left[\mu_N(p_j) \right] \quad \forall\, j \tag{5}$$

where $\mathbb{P}_{\mathbf{c},\mathbf{d}}$ denotes the set of all possible paths p_j. The probability measure that a voxel $\mathbf{x}$ belongs to a vessel is hence:

$$P_{\text{Vessel}}(\mathbf{x}) = \max_{\mathbf{s}_i \in \mathbb{O}} \left[\mu_K(\mathbf{x}, \mathbf{s}_i) \right] \quad \text{with} \quad P_{\text{Vessel}}(\mathbf{s}_i) = 1 \ \ \forall\, i \tag{6}$$

Note that this probability measure P_{Vessel} does not conform to the strict definition of a probability function. Even if P_{Vessel} drops below 0.5 for a voxel, this voxel can still belong most likely to the vascular tree. An appropriate threshold has to be chosen for binarization.

2.3.2 Probability Function

The local affinity $\mu_\kappa(\mathbf{c}, \mathbf{d})$ in Section 2.3.1 describes the likelihood that two neighboring voxels $\mathbf{c}, \mathbf{d}$ belong to the same class. Such a function typically considers the image content based on an intensity or gradient-based probability function, or a combination of both. Probability functions include, but are not limited to, the following [19]:

$$g_1(f(\mathbf{c}), f(\mathbf{d})) = e^{-\frac{1}{2\sigma_1^2}\left(\frac{f(\mathbf{c})+f(\mathbf{d})}{2}-\mu_1\right)^2} \tag{7}$$

$$g_2(f(\mathbf{c}), f(\mathbf{d})) = e^{-\frac{1}{2\sigma_2^2}(|f(\mathbf{c})-f(\mathbf{d})|-\mu_2)^2} \tag{8}$$

In these expressions, μ_1, μ_2 and σ_1^2, σ_2^2 represent the mean and variance of the expected object input values and their gradient magnitudes. In other words, g_1 and g_2 become large if the input value of $\frac{f(\mathbf{c})+f(\mathbf{d})}{2}$ and the gradient magnitude $|f(\mathbf{c}) - f(\mathbf{d})|$ are similar to the expected values μ_1 and μ_2, respectively. The parameters σ_1 and σ_2 control how fast the probability functions drop towards zero for values distant from the expected ones.

In the context of pulmonary vessel segmentation, the intensity-based probability function (7) (see Figure 4a) has proven to yield good segmentation results (see Section 3) while a gradient-based function tends to leak into non-vessel structures before segmenting the vascular tree accurately. One reason might be that the vessel boundaries appear slightly blurred due to partial volume effects and that hence the gradient between neighboring voxel is not as high as expected. Once the segmentation has leaked into the lung, a gradient-based function will cause the segmentation process to grow very fast into the mostly homogenous background.

The expected intensity value μ_1 in (7) is estimated from the input data by averaging the intensity values of all seed positions $\mathbf{s}_i$. Using this estimate rather than a pre-defined value considers intensity variations between different patients caused by, for example, the contrast agent used and bolus phase. The variance is set to a defined value, e.g., $\sigma_1 = 250$. However, the choice of σ_1 is not crucial in this setting, since it can be regarded as a normalization constant with respect to image noise within the object of interest.

While the above probability functions solely consider the input data, higher-level knowledge might be additionally encoded into this framework. For instance, similar to [6], voxels in close spatial proximity to the airway lumen might be considered as the airway wall, and hence should receive a low vessel probability (see Fig. 4b). Such a priori knowledge can be described by Equation (9), using a distance map that contains as input data the smallest Euclidean distance to the airway lumen.

$$g_3(\mathbf{c}) = 1 - e^{-\frac{1}{2\sigma_3^2}d(\mathbf{c})^2} \tag{9}$$

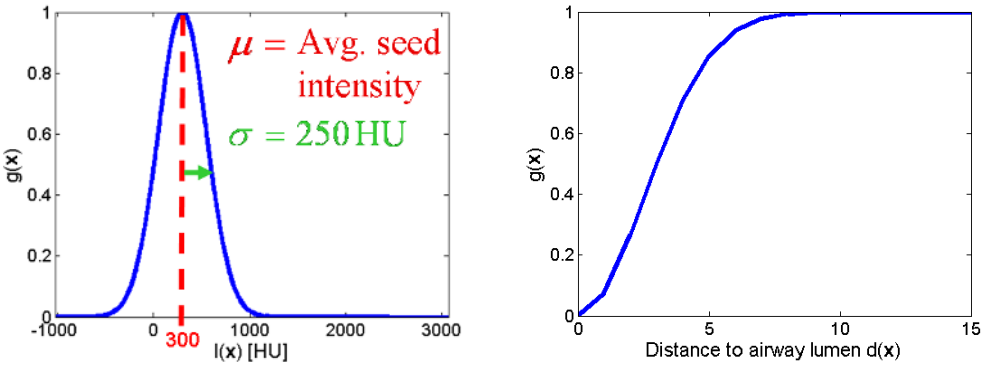

(a) Intensity-based (b) Distance-based

Figure 4. Probability functions that can be used to define the local affinity $\mu_\kappa(\mathbf{c}, \mathbf{d})$.

2.4 Manual Intervention

The possibilities for a user to interact with the described system are primarily twofold. First, the output of the fuzzy segmentation step reflects the probability that a voxel belongs to a vessel. For a binary classification an additional threshold has to be applied to obtain an unambiguous assignment of each voxel to the foreground (vessel) and background classes. This threshold strongly influences the sensitivity and specificity of the system. A high threshold (only voxels with a high vessel probability are considered to belong to a vessel) will result in a core vessel segmentation with a high specificity, but low sensitivity. On the other hand, a low threshold might result in over-segmentations and consequently a high sensitivity but lower specificity. This behavior can be interactively adjusted based on the segmentation output and the application-specific requirements.

Second, in the case of missing components or subtrees due to insufficient seed-point detection, additional seed positions can be manually defined, or wrongly located seed-points can be deleted. Moreover, in the presence of leakage into surrounding structures, such as the SVC or pathologies (e.g., lung nodules), further seed positions indicating background (non-vessel structures) might also be defined. Then, by using an appropriate probability function (see also Section 2.3.2), the probability of voxels belonging to other structures can be calculated. In that way, seed-points of different classes could compete among themselves to have voxels as their members. One possible realization is described in [20] as iterative relative fuzzy connectedness.

3. RESULTS

The proposed system has been evaluated on several contrast-enhanced chest CT scans from clinical PE cases and demonstrates overall promising results. These datasets were acquired using Siemens Sensation 16/64 scanners. The voxel size ranged from 0.559 to 0.723 mm in the axial plane and $0.6-0.7$ mm in the z-direction. The number of slices ranged from 372 to 540, with a slice thickness from 0.6 to 1.25 mm. For quantitative validation, manually selected region of interests (ROI) of size 50^3 voxels were semi-automatically segmented using the random walker algorithm [21], which has been demonstrated to yield accurate results for validation purposes [22]. These semi-automatic segmentations formed the ground truth voxels, in order to measure the true and false positive vessel detections.

In the examples shown in Fig. 5, a fully automatic approach was used and the resulting probability map was converted into a binary segmentation using different pre-defined thresholds. While a high threshold (Fig. 5a) results in a high segmentation specificity (mainly major vessels are included), a decrease of the threshold (Fig. 5b-c) increases the segmentation sensitivity and hence results in the inclusion of smaller vessels. The receiver operating characteristic (ROC) curves for three randomly selected ROIs of different lung regions are shown in Fig. 5d for varying thresholds. The corresponding pairs of sensitivity (ratio of truly positive segmented voxels to all object voxels) and specificity (ratio of truly negative segmented voxels to all background voxels) for the thresholds used for Fig. 5a-c are marked on each curve.

To examine the influence of the distance-based probability function (see Section 2.3.2) we have selected 20 ROIs from 10 patients including major airways in close proximity to the hilum. These have been used as a ground truth to validate the proposed system, using the intensity-based probability function alone

$$\mu_\kappa(\mathbf{d}, \mathbf{c}) = g_1(f(\mathbf{c}), f(\mathbf{d})) \tag{10}$$

and a combination of intensity and distance-based probability functions

$$\mu_\kappa(\mathbf{d}, \mathbf{c}) = g_1(f(\mathbf{c}), f(\mathbf{d})) \cdot \min\left(g_3(\mathbf{c}), g_3(\mathbf{d})\right) \tag{11}$$

for varying σ_3. The segmentation results in regions distant from major airways are not influenced by the distance-based probability function, and hence are not considered for this comparison. The best results could be obtained when designing g_3 in such a way that $g_3 = 0.5$ for $d = 3$ voxels from the airway lumen ($\sigma_3 = 2.55$). In other words, the fuzzy connectedness region growing speed decreases by 50% at an Euclidean distance of three voxels from the airway lumen. The improvement of segmentation accuracy using the combined function (black curve) compared to the intensity-based function alone (gray curve) is exemplarily shown in Fig. 6a based on two different patients. These ROC curves show the validation results of two ROIs for each patient while for patient 1 (solid lines) the

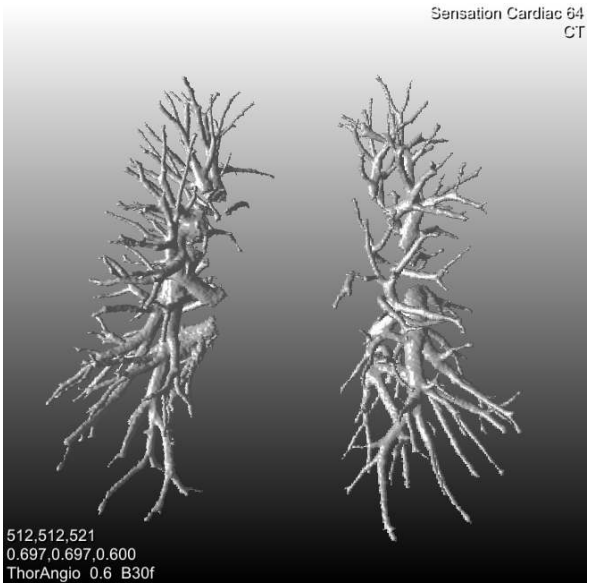

(a) $P_{Vessel} > 0.75$

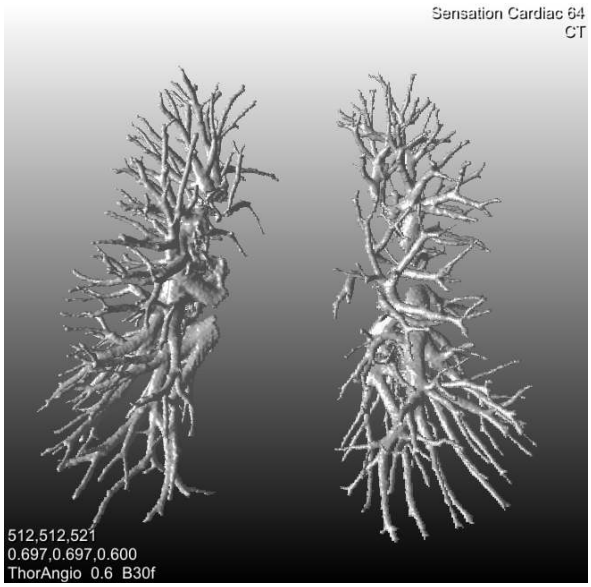

(b) $P_{Vessel} > 0.50$

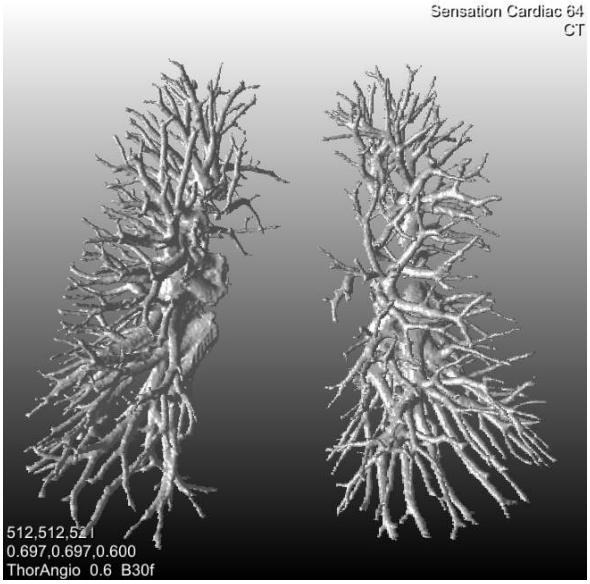

(c) $P_{Vessel} > 0.25$

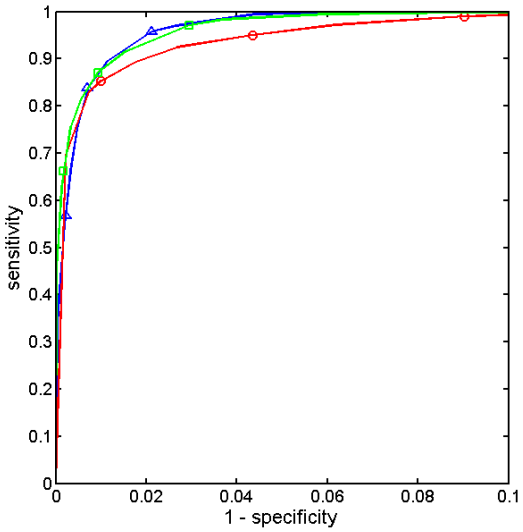

(d) Receiver operating characteristic (ROC)

Figure 5. 3D renderings of the segmentation results of the proposed system. Subfigures (a)-(c) show only voxels with a probability P_{Vessel} larger than the threshold specified in the caption, thus resulting in different segmentation sensitivities and specificities. Note that the probability P_{Vessel} does not conform to the typical definition of a probability function. Even if P_{Vessel} drops below 0.5 for a voxel, this voxel is still likely to belong to the vascular tree. Subfigure (d) exemplarily shows the validation results of the proposed method compared to three randomly selected and semi-automatically segmented sub-volumes of size $50 \times 50 \times 50$ voxels of different lung regions. For each sub-volume the ROC curve is visualized across different thresholds, including those used in Subfigures (a)-(c), which correspond to the marked positions on each curve.

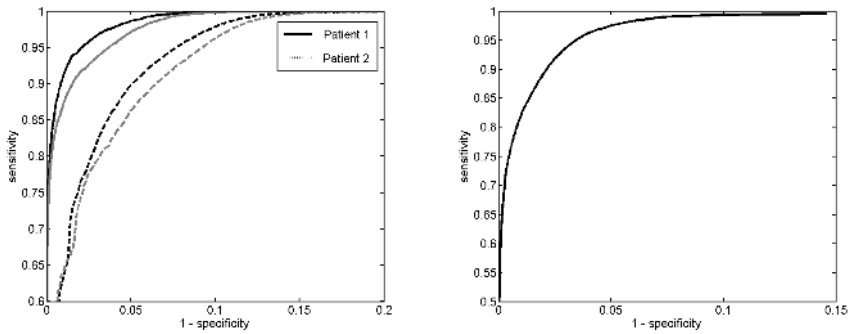

(a) Comparison of different functions (b) Overall results

Figure 6. (a) ROC curves comparing different functions for the local affinity $\mu_\kappa(\mathbf{c}, \mathbf{d})$ and (b) the overall results based on 58 randomly placed ROIs from 10 patients.

segmentation accuracy was very high, and for patient 2 (dashed lines) the algorithm did not perform as well. In general, the combined function was superior to the intensity-based function alone. Fig. 7 shows exemplarily the segmentation results for identical thresholds ($P_{Vessel} > 0.4$). Using the intensity-based function alone (left) results in a leakage into the airway wall that is avoided by combining it with the distance-based function (right). The sensitivity increases up to 5.5% at constant specificity. In some regions however, both methods provide comparable results, while in one out of twenty regions, the segmentation accuracy was significantly decreased.

For the overall validation of the proposed method, a total of 58 ROIs from 10 patients were randomly selected from all lung regions, including small as well as large vessels. The segmentation was conducted using the local affinity as described in Equation (11). Observing the ROC curve in Fig. 6b, one can see that the sensitivity of the method equals 89% at a specificity level of 98%, using a threshold of $P_{Vessel} > 0.4$, which segments the vessels relevant for PE applications consistently well. Further examples are shown in Fig. 8. Using this pre-defined threshold results in a Dice similarity coefficient (DSC) [23]

$$DSC = \frac{2 \cdot TP}{2 \cdot TP + FP + FN} = 84.6\% \tag{12}$$

with TP, FP, and FN being the true positive, false positive, and false negative voxel count. The average processing time was determined to be 38.04s on 10 patients with already existing lung segmentations on a standard PC (Pentium 4, 3.4GHz). Note that the methods have not yet been optimized in terms of computational efficiency.

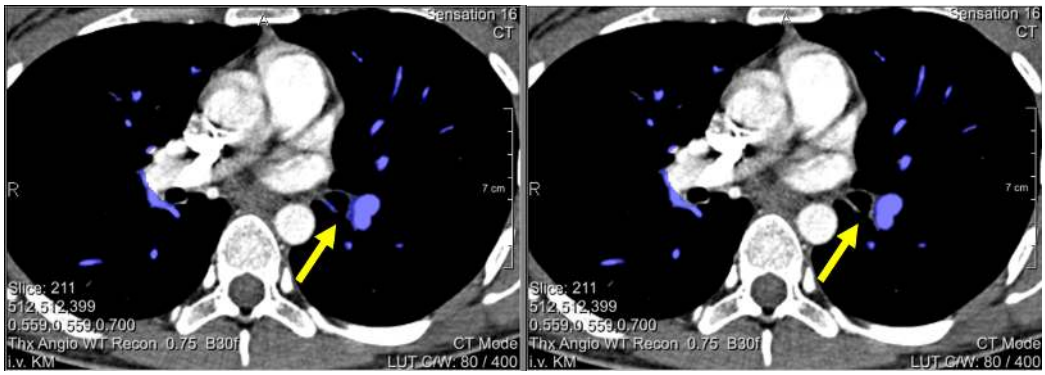

Figure 7. Segmentation results using different functions for local affinity. The left image shows the binary vessel segmentation (blue overlay) using the intensity-based probability function, which has leaked into the airway wall. With identical threshold ($P_{Vessel} > 0.4$), but a combination of intensity and distance-based probability function instead, the leakage into airway walls is significantly reduced (best viewed in color).

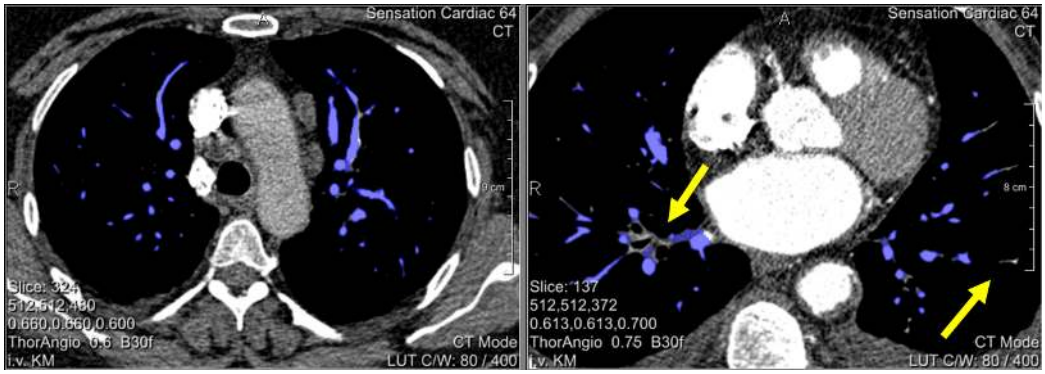

Figure 8. Further segmentation results using $P_{Vessel} > 0.4$. Left: Large as well as small vessels are segmented accurately. Right: Example for which the algorithm performed not that well. Smaller vessels are missed while leaking into non-vessel structure in close proximity to larger vessels (best viewed in color).

4. CONCLUSION

We have presented a flexible system for automatic lung vessel segmentation in contrast enhanced CT data that can be used for different applications. The system combines the strengths of both threshold and seed-point based methods, resulting in a robust segmentation without any user interaction. Multiple seed-points within the lung segmentation mask are identified using a threshold-based approach. In that way, all subtrees within each lung area are identified, even if the vascular tree has already bifurcated before entering the segmented lung regions. Furthermore, in the presence of a PE within a larger artery, the successor subtrees are separately identified as long as the PE is non-blocking and hence are not completely lost even if the PE (or any other local inhomogeneity) would cause a seed-point based segmentation algorithm alone to terminate early.

Next, the fuzzy connectedness algorithm is utilized to calculate the probability of each voxel belonging to the vascular tree. Therefore the segmentation sensitivity/specificity trade-off of the system can be easily adjusted to the requirements of the specific application by simply adjusting the threshold that converts the probability map into a binary segmentation. Additionally the system allows for convenient user interaction to modify the segmentation outcome by specifying further seed positions.

The method has been evaluated on CT scans from clinical PE cases and demonstrates overall promising results. Using a pre-defined threshold that provides consistent results relevant for PE applications, the sensitivity of the method was determined to be 89% at a specificity level of 98%. Analyzing the results shows that the method still tends to leak into non-vessel structures in close proximity to larger vessels prior to capturing small vessels. Hence, future work will include locally adapting the segmentation parameters.

Although these methods have been primary applied to the lung region, they could also be used for vessel segmentation in other regions or organs using CT data or any preprocessed data, such as the output from vessel enhancement filters, such as described in [8, 9]), or combinations, resulting in multimodal images. The methods may also be applicable to other modalities, such as MRA data.

REFERENCES

1. A. P. Kiraly, E. Pichon, D. P. Naidich, and C. L. Novak, "Analysis of arterial subtrees affected by pulmonary emboli," in *Medical Imaging 2004: Image Processing. Procs of the SPIE*, **5370**, pp. 1720–1729, May 2004.
2. C. Wu, G. Agam, A. S. Roy, and S. G. Armato, III, "Regulated morphology approach to fuzzy shape analysis with application to blood vessel extraction in thoracic CT scans," in *Medical Imaging 2004: Image Processing. Procs of the SPIE*, **5370**, pp. 1262–1270, May 2004.
3. H. Shikata, E. A. Hoffman, and M. Sonka, "Automated segmentation of pulmonary vascular tree from 3D CT images," in *Medical Imaging 2004: Physiology, Function, and Structure from Medical Images. Procs of the SPIE*, **5369**, pp. 107–116, Apr. 2004.

4. C. Zhou, H.-P. Chan, L. M. Hadjiiski, S. Patel, P. N. Cascade, B. Sahiner, J. Wei, J. Ge, and E. A. Kazerooni, "Automatic pulmonary vessel segmentation in 3D computed tomographic pulmonary angiographic (CTPA) images," in *Medical Imaging 2006: Image Processing. Procs of the SPIE*, **6144**, pp. 1524–1530, Mar. 2006.
5. T. Buelow, R. Wiemker, T. Blaffert, C. Lorenz, and S. Renisch, "Automatic extraction of the pulmonary artery tree from multi-slice CT data," in *Medical Imaging 2005: Physiology, Function, and Structure from Medical Images. Procs of the SPIE*, **5746**, pp. 730–740, Apr. 2005.
6. X. Zhou, T. Hayashi, T. Hara, H. Fujita, R. Yokoyama, T. Kiryu, and H. Hoshi, "Automatic segmentation and recognition of anatomical lung structures from high-resolution chest CT images," *Computerized Medical Imaging and Graphics* **30**, pp. 299–313, 2006.
7. H. Zhang, Z. Bian, D. Jiang, Z. Yuan, and M. Ye, "Level set method for pulmonary vessels extraction," in *IEEE International Conference on Image Processing. ICIP*, pp. II: 1105–1108, 2003.
8. A. F. Frangi, W. J. Niessen, K. L. Vincken, and M. A. Viergever, "Multiscale Vessel Enhancement Filtering," *Lecture Notes in Computer Science* **1496**, pp. 130–137, 1998.
9. Y. Sato, S. Nakajima, N. Shiraga, H. Atsumi, S. Yoshida, T. Koller, G. Gerig, and R. Kikinis, "Three-dimensional multi-scale line filter for segmentation and visualization of curvilinear structures in medical images," *Medical Image Analysis* **2**(2), pp. 143–168, 1998.
10. S. Aylward and E. Bullitt, "Initialization, noise, singularities, and scale in height ridge traversal for tubular object centerline extraction," *IEEE Transactions on Medical Imaging* **21**, pp. 61–75, 2002.
11. S. Eiho, H. Sekiguchi, T. Sugimoto, and S. Urayama, "Branch-based Region Growing Method for Blood Vessel Segmentation," in *XXth ISPRS Congress*, pp. 796–801, ISPRS, 2004.
12. C. Zhou, H.-P. Chan, L. M. Hadjiiski, A. Chughtai, S. Patel, P. N. Cascade, B. Sahiner, J. Wei, J. Ge, and E. A. Kazerooni, "Automated detection of pulmonary embolism (PE) in computed tomographic pulmonary angiographic (CTPA) images: multiscale hierachical expectation-maximization segmentation of vessels and PEs," in *Medical Imaging 2007: Computer-Aided Diagnosis. Procs of the SPIE*, **6514**, Mar. 2007.
13. G. Agam, S. G. Armato III, and C. Wu, "Vessel tree reconstruction in thoracic CT scans with application to nodule detection.," *IEEE Transactions on Medical Imaging* **24**(4), pp. 486–499, 2005.
14. S. Hu, E. Hoffman, and J. Reinhardt, "Automatic lung segmentation for accurate quantitation of volumetric x-ray ct images," *IEEE Transactions on Medical Imaging* **20**, pp. 490–498, June 2001.
15. A. P. Kiraly, W. E. Higgins, E. A. Hoffman, G. McLennan, and J. M. Reinhardt, "3D human airway segmentation for virtual bronchoscopy," in *Medical Imaging 2002: Physiology and Function from Multidimensional Images, Procs of the SPIE*, **4683**, pp. 16–29, Apr. 2002.
16. I. Sluimer, A. Schilham, M. Prokop, and B. van Ginneken, "Computer analysis of computed tomography scans of the lung: A survey," *IEEE Transactions on Medical Imaging* **25**(4), pp. 385–405, 2006.
17. J. K. Udupa and P. K. Saha, "Fuzzy connectedness and image segmentation.," *Procs of the IEEE* **91**(10), pp. 1649–1669, 2003.
18. J. Tschirren, E. A. Hoffman, G. McLennan, and M. Sonka, "Segmentation and Quantitative Analysis of Intrathoracic Airway Trees from Computed Tomography Images," *Proc Am Thorac Soc* **2**(6), pp. 484–487, 2005.
19. J. K. Udupa and S. Samarasekera, "Fuzzy connectedness and object definition: theory, algorithms, and applications in image segmentation," *Graph. Models Image Process.* **58**(3), pp. 246–261, 1996.
20. J. K. Udupa, P. K. Saha, and R. A. Lotufo, "Relative fuzzy connectedness and object definition: Theory, algorithms, and applications in image segmentation," *IEEE Transactions on Pattern Analysis and Machine Intelligence* **24**(11), pp. 1485–1500, 2002.
21. L. Grady, T. Schiwietz, S. Aharon, and R. Westermann, "Random Walks for Interactive Organ Segmentation in Two and Three Dimensions: Implementation and Validation," in *MICCAI, LNCS 3750*, pp. 773–780, Oct. 2005.
22. J. N. Kaftan, A. Bakai, F. Maier, and T. Aach, "Semi-automatic pulmonary vessel segmentation in CT data as reference to validate automatic approaches (German)," in *Bildverarbeitung für die Medizin*, 2008. to appear.
23. K. H. Zou, S. K. Warfield, A. Bharatha, C. M. Tempany, M. R. Kaus, S. J. Haker, W. M. Wells, F. A. Jolesz, and R. Kikinis, "Statistical validation of image segmentation quality based on a spatial overlap index," in *Acad Radiol.*, **11**, pp. 178–189, Feb. 2004.